Impact of pore size on the vascularization and osseointegration of ceramic bone substitutes *in vivo*

Frank M. Klenke,[1,2] Yuelian Liu,[3,4] Huipin Yuan,[5] Ernst B. Hunziker,[4] Klaus A. Siebenrock,[2] Willy Hofstetter[1]

[1]*Department Clinical Research, Group for Bone Biology and Orthopedic Research, University of Berne, CH-3010 Berne, Switzerland*

[2]*Department of Orthopedic Surgery, Inselspital, University of Berne, CH-3010 Berne, Switzerland*

[3]*Section of Oral Implantology and Prosthetic Dentistry, Department of Oral Function, Academic Center for Dentistry Amsterdam (ACTA), NL-1066 EA Amsterdam, The Netherlands*

[4]*ITI Research Institute for Dental and Skeletal Biology, University of Berne, CH-3010 Berne, Switzerland*

[5]*Progentix BV, Prof. Bronkhorstlaan 10, NL-3723 MB Bilthoven, The Netherlands*

Received 18 February 2007; revised 25 May 2007; accepted 7 June 2007
Published online 26 September 2007 in Wiley InterScience (www.interscience.wiley.com). DOI: 10.1002/jbm.a.31559

Abstract: The repair of bone defects with biomaterials depends on a sufficient vascularization of the implantation site. We analyzed the effect of pore size on the vascularization and osseointegration of biphasic calcium phosphate particles, which were implanted into critical-sized cranial defects in *Balb/c* mice. Dense particles and particles with pore sizes in the ranges 40–70, 70–140, 140–210, and 210–280 μm were tested ($n = 6$ animals per group). Angiogenesis, vascularization, and leukocyte–endothelium interactions were monitored for 28 days by intravital microscopy. The formation of new bone and the bone–interface contact (BIC) were determined histomorphometrically. Twenty-eight days after implantation, the functional capillary density was significantly higher with ceramic particles whose pore sizes exceeded 140 μm [140–210 μm: 6.6 (±0.8) mm/mm^2; 210–280 μm: 7.3 (±0.6) mm/mm^2] than with those whose pore sizes were lesser than 140 μm [40–70 μm: 5.3 (±0.4) mm/mm^2; 70–140 μm: 5.6 (±0.3) mm/mm^2] or with dense particles [5.7 (±0.8) mm/mm^2]. The volume of newly-formed bone deposited within the implants increased as the pore size increased [40–70 μm: 0.07 (±0.02) mm^3; 70–140 μm: 0.10 (±0.06) mm^3; 140–210 μm: 0.13 (±0.05) mm^3; 210–280 μm: 0.15 (±0.06) mm^3]. Similar results were observed for the BIC. The data demonstrates pore size to be a critical parameter governing the dynamic processes of vascularization and osseointegration of bone substitutes. © 2007 Wiley Periodicals, Inc. J Biomed Mater Res 85A: 777–786, 2008

Key words: bone substitute; histomorphometry; intravital microscopy; osseointegration; vascularization

INTRODUCTION

Skeletal defects generated by the resection of bone tumors or by trauma are usually reconstructed with autologous grafts of cortical or cancellous bone harvested from the iliac crest. However, the harvest of bone from an autologous source is disadvantageous in several respects: the supply of material is limited, its excision is associated with donor-site morbidity, and the procedure prolongs the time of surgery.[1] Consequently, there is a growing interest in the development of biomaterials that can integrate with existing bone, can be turned over, and be subsequently replaced by newly-formed osseous tissue. Vascularization is crucial for the development and the repair of most tissues, and is a precondition for the healing of bone defects.[2–4] Revascularization of the implantation site ensures an adequate supply of nutrients, the prompt removal of metabolic by-products, and the delivery of cells and growth factors that support the formation of osseous tissue. It is thus crucial for the remodeling of bone substitutes and their replacement with osseous tissue.

The dynamics and the extent of bone ingrowth into porous calcium phosphate ceramics are known to depend upon the pore size of the material.[5–10]

No benefit of any kind will be received either directly or indirectly by the authors.

Correspondence to: F.M. Klenke; e-mail: frank.klenke@dkf.unibe.ch

Contract grant sponsor: AO Research Foundation, Dübendorf, Switzerland; contract grant number: 05-K82
Contract grant sponsor: Novartis Foundation for Medicine and Biology, Basel, Switzerland; contract grant number: 05B35
Contract grant sponsor: Department Clinical Research, University of Berne, Berne, Switzerland

Furthermore, bone substitutes with an interconnected system of pores can be invaded by blood vessels, enabling the development of a dense vascular meshwork. We therefore hypothesized that the pore size of bone substitutes influences the ingrowth not only of osseous tissue but also of capillary sprouts, and thus angiogenesis, thereby impacting the healing process after implantation.

Intravital microscopy permits a quantitative as well as a qualitative analysis of angiogenesis, the microcirculation, microvascular perfusion, leukocyte–endothelium interaction (LEI), and endothelial leakage.[11–13] The method has been used to investigate the cerebral microcirculation in rats and the angiogenesis of malignant cranial tumors in mice.[14–19] Although the cranium has been used as an implantation site for bone substitutes in rodents,[20–22] intravital microscopy has not been applied to investigate the angiogenesis and microcirculation of the implanted biomaterials.

The aim of the present study was to evaluate the influence of the pore size of a particulate calcium phosphate ceramic on vascularization and bone formation within critical-sized cranial defects in mice. Vascularization was quantified by intravital microscopy and bone formation by histomorphometry.

MATERIALS AND METHODS

Preparation of the ceramic bone substitute with different pore sizes

Porous, biphasic calcium phosphate ceramics composed of 80% hydroxyapatite and 20% β-tricalcium phosphate were prepared from calcium phosphate apatite powder with a calcium phosphate ratio of 1.66. First, porous green bodies were prepared from the apatite powder by adding 0.5% hydrogen peroxide solution and naphthalene particles (Fluka Chemie, Zwijndrecht, The Netherlands) at 60°C. The naphthalene particles and the aqueous phase were subsequently evaporated at 80°C. Porous calcium phosphate ceramics were obtained by sintering the dried porous green bodies at 1150°C for 8 h.[23–25]

Different pore sizes were generated using naphthalene particles of different sizes: (i) naphthalene particles with sizes of 300–400 μm generated pores in the size range 210–280 μm; (ii) naphthalene particles with sizes of 212–300 μm generated pores in the size range 140–210 μm; (iii) naphthalene particles with sizes of 106–212 μm generated pores in the size range 70–140 μm; and (iv) naphthalene particles with sizes of 75–106 μm generated pores in the size range 40–70 μm. The overall porosity of the ceramic bodies was 75% (±5%) [macropores (>10 μm): approximately 50%; micropores (0.1–10 μm): approximately 25%].

A dense ceramic body was prepared by mixing the apatite powder with 0.5% hydrogen peroxide solution in the absence of naphthalene particles. This material manifested no macroporous structure. Micropores (0.1–10 μm) were engendered by the presence of hydrogen peroxide.

For each of the five groups, ceramic particles with sizes of 0.5–1.0 mm were prepared from the ceramic bodies, cleaned, and autoclaved at 121°C for 30 min prior to use.

Preparation of cranial-window defects

Thirty-six 8-week-old male *Balb/c* mice (BALB7cAnNCrl; Charles River Wiga, Germany) were used for this study, which was approved by the local committee for animal experimentation (BVET, Berne, Switzerland) and conducted in accordance with its regulations.

Cranial-window defects were created in the calvariae for the implantation of the ceramic particles. The animal model followed previously described cranial window preparations applied to investigate the cerebral microcirculation and the microcirculation of malignant tumors in mice.[14,26–29] All surgical procedures were performed within a laminar-flow unit under strictly aseptic conditions. The mice were anaesthetized with a mixture of fentanyl (50 μg/kg of body weight), medetomidine (500 μg/kg of body weight), and climazolame (5 mg/kg of body weight), which was injected intraperitoneally. After shaving and disinfection of the scalp with 70% ethanol, the mice were secured within a custom-made stereotactic device. An oval area of the scalp (~15 × 10 mm^2) was removed to expose the frontal and parietal bones with the coronal, lambdoid and sagittal sutures [Fig. 1(A)]. Using a dental drilling device (Nouvag MD 10, Nouvag AG, Switzerland), a circular, 4-mm-diameter defect was generated within the calvarium, leaving only a thin layer of the internal tabula in place. The latter was then carefully lifted with a pair of fine forceps. After dividing the adhesions which attach the internal tabula to the sagittal sinus, the former was completely removed to create a full-thick-

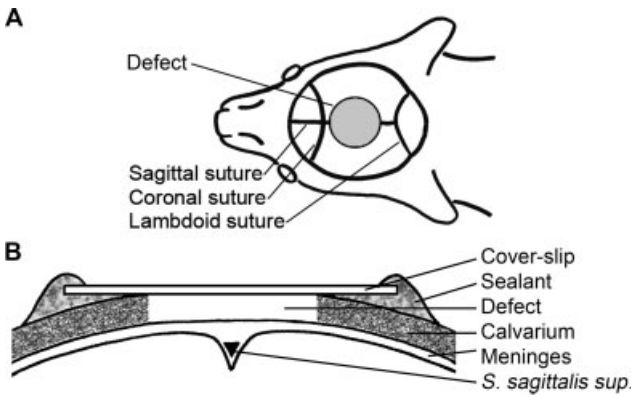

Figure 1. (A) Scheme of the cranial-window preparation (viewed from above), depicting the circular, 4-mm-diameter defect and its relationship to the sagittal, coronal and lamboid sutures. (B) Schematic, cross-sectional view of the cranial full-thickness defect. The exposed meninges were preserved intact, to avoid angiogenesis from the underlying blood vessels. The site was covered with a glass cover slip, which was sealed with a suitable adhesive ("Sealant").

ness defect [Fig. 1(B)]. Care was taken to avoid mechanical or thermal damage to the dura mater and the underlying brain tissue. If this occurred, the animal was killed immediately and excluded from the study. If bleeding from the bone occurred, the surgical procedure was interrupted to clear the site by swabbing with a sterile Q-tip. Ceramic particles from one of the five pore-size categories ($n = 6$ for each group) were then implanted within the defect. A control group was established, in which the defects were left empty ($n = 6$). To protect the tissue from dehydration and mechanical damage, the exposed site was covered with a circular, 7-mm-diameter glass slip (Assistent, Germany), which was secured to the bone margin with cement (a mixture of ethylcyanoacrylate glue; Pattex®; Blitz Kleber, Henkel, Germany; and a methylmethacrylate polymer; GC Ostron®-powder; GC Europe, Belgium).

Intravital microscopy

During the first week of implantation, the defect site was monitored every 12 h using a stereotactic microscope under vertical illumination. The time at which newly-formed blood vessels invaded the implanted biomaterial was noted.

Intravital fluorescence video-microscopy was performed 7, 14, 21, and 28 days after implantation using a vertical illumination fluorescence microscope unit (Zeiss Axioplan 2, Zeiss, Germany) equipped with −2.5× and −20× objectives and with fluorescence filter systems for green and blue light. For the offline analysis, regions of interest were recorded on video-tapes using an S-VHS videocassette recorder, which was connected to a digital microscope camera. The microcirculation was rendered visible by an intravenous injection of the plasma marker fluorescein–isothiocyanate-labeled dextran (FD 2000S; Sigma Aldrich; 60 μL of a 5% solution in 0.9% saline). The interaction between leukocytes and the vascular endothelium was visualized by an intravenous injection of the leukocyte marker rhodamin 6G (R4127, Sigma Aldrich; 90 μL of a 0.05% solution in 0.9% saline).

Offline analysis of vascularization, microhemodynamic variables, and LEI

The functional capillary density (FCD) within the implantation site was defined as the total length of the erythrocyte-perfused nutritive capillaries (in mm) per two-dimensional defect surface (in mm^2). This parameter has been well established as a measure of the microvascular perfusion in various tissues.[30–33] The offline analysis of FCD was performed on digital fluorescence images using Simple PCI software (Version 6.0, Compix Inc, Imaging Systems, Cranberry Township, USA).

Microhemodynamic parameters and the LEI were analyzed on digital images of the regions of interest. Six to eight such regions were evaluated per animal and per time point. The implantation site was divided into four quarters. Two regions of interest in each of the four fields were photographed: one in the periphery and one in the centre.

Inconsistencies in microhemodynamic variables can arise from changes in the mechanical or the morphological properties of the vessels.[34] To avoid this problem, 100-μm-long segments of vessel with similar diameters and running were analyzed per animal and per time point. Each of these regions was monitored for 30 s for the measurements of microhemodynamic variables and for the evaluation of LEI. Vessel diameters (D), were measured perpendicular to the vessel path and expressed in micrometers. The centreline velocity of the blood stream (v_{centre}) was determined by measuring the length (L) within a vessel segment over which leukocytes coursed within a defined time (t): $v_{centre} = L/t$ (μm/s). Leukocytes were classified as free-floating, rolling, or sticking according to their interactions with the microvascular endothelium. The number of sticking leukocytes (N_{Sti}) was expressed as the numerical density of cells (WBC_{Sti}) that adhered firmly to the inner surface of the investigated 100-μm-long vessel segment during the 30-s observation period: $WBC_{Sti} = N_{Sti} \times 10^6/[\text{pi}\ (\pi) \times D \times 100]$ (cells/mm^2). Rolling leukocytes are defined as a population of cells that interacts transiently with the vessel wall, and that have a velocity at least 50% lower than v_{centre}. The rolling count (WBC_{Rol}) was expressed as: $WBC_{Rol} = (N_{Rol}/N_{Flo}) \times 100$ (%), where N_{Rol} is the number of rolling leukocytes and N_{Flo} is the number of free-floating ones. Leukocyte flux (WBC_{Flux}) was defined as the number of free-floating leukocytes that passed a vessel cross-section within a certain time. Leukocyte flux was normalized for the cross-sectional area of the observed microvessel and the observation time (t): $(WBC_{Flux}) = N_{Flo} \times 10^6/[(D/2)^2 \times \pi \times t]$ (cells/mm^2/s). The apparent shear rate of the vessel wall (γ) was derived from Poiseuille's law for a Newtonian fluid: $\gamma = (v_{centre}/D) \times 8$ (1/s).[35] Blood flow (Q) was calculated as: $Q = v_{centre} \times D^2 \times [\pi]/4000$ (pl/s).

TABLE I
Time After Implantation at Which Vessels First Penetrated the Ceramic Materials With Different Pore Sizes

Pore Size (μm)	First Appearance of Vessels (hours after implantation)
210–280	$106 \pm 14^{\#,*,**}$
140–210	$111 \pm 11^{\#,*,**}$
70–140	132 ± 10
40–70	135 ± 9
Dense ceramics	141 ± 13
Control (no ceramic)	132 ± 17

Angiogenesis within the implantation site was investigated using intravital microscopy. The appearance of newly formed vessels was observed at 12-h intervals.

Mean values ± standard deviation are represented ($n = 6$ for each group).

$^{\#}p < 0.05$ vs. dense ceramics.

$^{*}p < 0.05$ vs. 40–70 μm.

$^{**}p < 0.05$ vs. 70–140 μm.

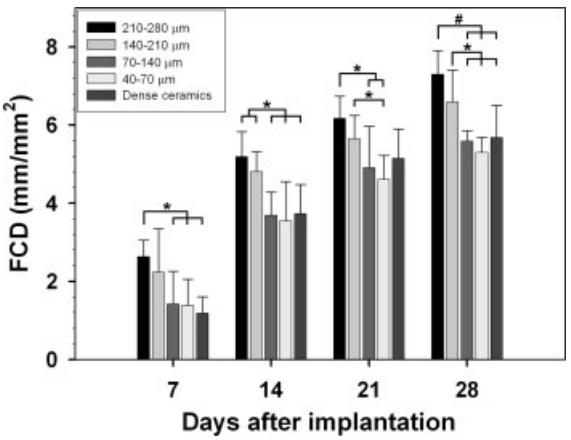

Figure 2. Vascularization of BCP ceramics was analyzed for 28 days by intravital microscopy. The graph depicts the FCDs of the ceramic materials with different pore sizes on days 7, 14, 21, and 28 after implantation. Mean values are represented together with the standard deviation ($n = 6$ for each group and time point). Statistically significant differences between the values in each group are indicated by the symbols "*" ($p < 0.05$) and "#" ($p < 0.001$).

Histomorphometry

At the end of the intravital observation period (28 days), the mice were killed with CO_2. The implanted material was immediately excised together with the surrounding calvarial and brain tissue for the histomorphometric analysis. Each specimen was chemically fixed in buffered 4% paraformaldehyde solution, dehydrated in ethanol, and embedded in methylmethacrylate according to the procedure described by Erben et al.[36] The embedded material was cut perpendicular to the sagittal plane according to a systematic random sampling protocol: 300-µm-thick sections, separated by a constant distance of 300 µm, were produced, with a random start within 200 µm of the left-hand margin of the defect. Each specimen yielded five serial sections. The sections were surface stained with McNeal's tetrachrome.[37,38]

The volume of newly-formed bone was quantified on light microscopic images of the sections using Cavalieri's method.[39] The surface area density of bone and the bone–interface contact (BIC) area were determined using the cycloid test system described by Baddeley et al.[40]

Statistics

All numerical data are presented as mean values together with the standard deviation. The data were statistically evaluated by ANOVA using SigmaStat® software for Windows (Version 3.01, Systat Software, San Jose, CA, USA). Pairwise multiple comparisons were made using the Student–Newman–Keuls method. Differences were considered to be statistically significant if the p-value was less than 0.05. For the statistical analysis of correlations, Pearson's product moment was calculated.

RESULTS

Vascularization of the ceramic material with different pore sizes

Angiogenic sprouting and the development of a vascular network were monitored by intravital microscopy. Vessel formation occurred significantly earlier in ceramic particles whose pore sizes exceeded 140 µm (pore sizes 140–210 µm: 111 ± 11 h; pore sizes 210–280 µm: 106 ± 15 h) than with particles whose pore sizes were smaller than 140 µm (pore sizes 40–70 µm: 135 ± 9 h; pore sizes 70–140 µm: 132 ± 10 h) or with dense particles (141 ± 13 h) (Table I).

TABLE II
Microhemodynamic Variables for Sprouting Vessels Penetrating the Ceramic Materials With Different Pore Sizes, 14 and 28 days after Implantation

Pore Size (µm)	Day after Implantation	Vessel Diameter (µm)	Centerline Velocity of Blood Stream (µm/s)	Blood Flow (pl/s)	Shear Rate of Vessel Wall (1/s)
Control (no ceramic)	14	32.9 ± 4.2	172.0 ± 51.5	157.6 ± 64.9	42.9 ± 14.0
	28	33.0 ± 5.7	224.3 ± 127.8	177.4 ± 67.2	63.3 ± 22.2
Dense ceramics	14	25.3 ± 3.7	160.7 ± 56.1	91.8 ± 64.6	52.2 ± 13.6
	28	30.4 ± 5.1	150.1 ± 15.4	116.2 ± 41.6	41.8 ± 8.7
40–70	14	30.1 ± 6.5	181.1 ± 56.6	143.7 ± 103.3	50.0 ± 16.3
	28	34.1 ± 9.4	173.8 ± 41.9	249.7 ± 119.0	46.7 ± 20.3
70–140	14	28.6 ± 4.7	126.1 ± 27.9	82.6 ± 27.4	37.3 ± 12.6
	28	26.8 ± 3.6	150.8 ± 54.0	92.2 ± 33.7	47.1 ± 19.4
140–210	14	26.3 ± 6.7	173.0 ± 47.8	99.6 ± 51.0	55.7 ± 15.4
	28	30.8 ± 3.2	154.8 ± 30.3	116.7 ± 18.8	42.3 ± 11.0
210–280	14	25.0 ± 4.5	122.1 ± 35.2	69.8 ± 33.9	39.5 ± 6.4
	28	30.5 ± 3.6	207.8 ± 53.7	158.7 ± 43.7	55.8 ± 20.6

The microhemodynamic variables were analyzed on days 14 and 28 by intravital microscopy on 6–8 vessel segments per time-point and animal. In none of the experimental groups did the values for any of the four parameters differ significantly from those in the control group at either of the two time-points. Mean values ± standard deviation are represented ($n = 6$ for each group and time-point).

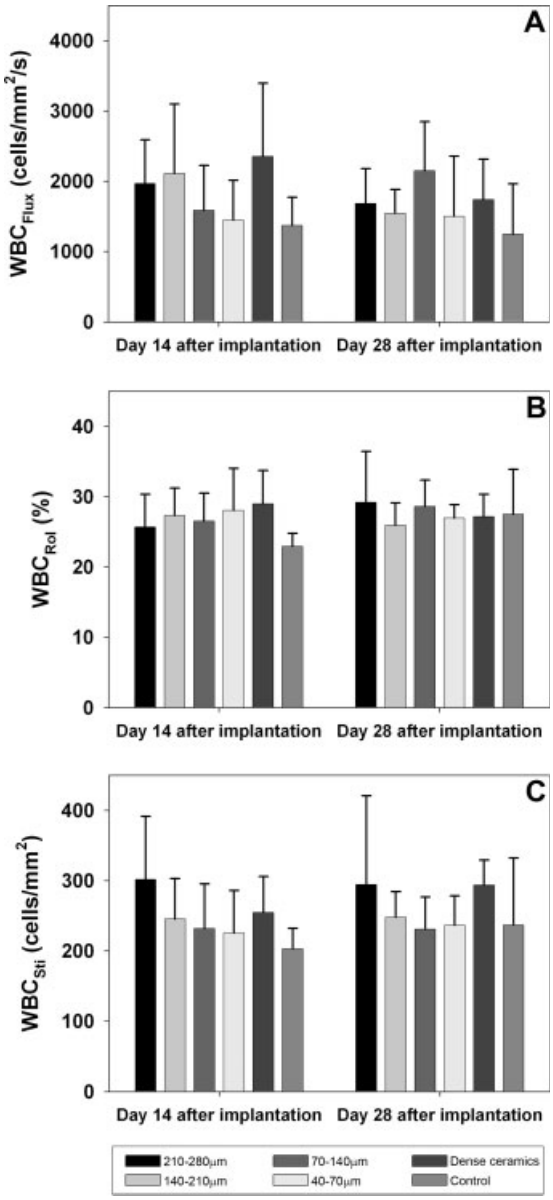

Figure 3. LEI was analyzed on days 14 and 28 to ascertain whether the ceramics elicited an immune response within the host tissue. (A) WBC_{Flux}: number of free-floating leukocytes that passed a vessel cross-section within a certain time. (B) WBC_{RoI}: number of rolling leukocytes divided by the number of free-floating ones. Rolling leukocytes are defined as a population of cells that interacts transiently with the vessel wall. (C) WBC_{Sti}: numerical density of leukocytes that attached firmly to the inner surface of the investigated 100-μm-long vessel segment during the 30-s observation period. Data are represented as mean values ± SD ($n = 6$ for each group and time point). In none of the experimental groups did the values for any of the three parameters differ significantly from those in the control group at either of the two junctures.

In the control (empty) defects, the first signs of vascularization were observed after 132 ± 17 h. In all groups, the capillary sprouts arose from vessels located within the surrounding bone.

Between the 7th and the 28th day of intravital observation, the FCD progressively increased in all groups (Fig. 2). By day 28, the FCD was higher in ceramic particles whose pore sizes exceeded 140 μm (pore sizes 140–210 μm: 6.6 ± 0.8 mm/mm^2; pore size 210–280 μm: 7.3 ± 0.6 mm/mm^2) than with either those whose pore sizes were smaller than 140 μm (pore sizes 40–70 μm: 5.3 ± 0.4 mm/mm^2; pore sizes 70–140 μm: 5.6 ± 0.3 mm/mm^2) or dense particles (5.7 ± 0.8 mm/mm^2). The FCDs for the two groups with pore sizes exceeding 140 μm did not differ significantly from each during the monitoring period (7–28 days). For the two groups with pore sizes smaller than 140 μm, the differences between the FCDs tended to increase with time, with higher values being registered for the larger (70–140 μm) than for the smaller (40–70 μm) ones. However, the differences did not attain statistical significance at any point in time.

Microhemodynamic variables and LEI

To ascertain whether the ceramic particles elicited an immune reaction within the host tissue, several microhemodynamic variables (Table II), as well as the LEI (Fig. 3), were determined on the 14th and the 28th days of intravital monitoring. In none of the groups were any of the parameters elevated above control values.

Bone formation

The volume of newly-formed bone (Table III) and the BIC (Table IV) were determined histomorphometrically 28 days after surgery for each of the five experimental groups and the control.

The volume of newly-formed bone deposited between the ceramic particles (V Bone ext. in Table III) was greater in each of the four porous-ceramic groups than in the dense-ceramic one. The volume of bone laid down within the pores of the ceramic material (V Bone pores in Table III) decreased with decreasing pore size. The values for the smallest and the largest pore sizes differed significantly from each other ($p < 0.05$; Table III). Similar trends were observed for the bone volume density (total volume of newly-formed bone divided by the volume of the defect from which the volume of the ceramic material has been subtracted) (Table III).

BIC was defined as the ratio of the ceramic surface that was covered with new bone to the total ceramic surface. The BIC for the internal (pore) surface of the ceramic particles was significantly larger in the two groups with pore sizes exceeding 140 μm than in either of the two groups with pore sizes less than

TABLE III
Absolute Volumes and Volume Density Ratios of Newly-Formed Bone Associated With the Ceramic Materials Bearing Pores of Different Sizes, 28 days after Implantation

Pore Size (μm)	V Def. (mm^3)	V Cer (mm^3)	V Pore (mm^3)	V Bone Ext. (mm^3)	V Bone Pores (mm^3)	V_v Bone Ext.	V_v Bone Pores
210–280	8.1 ± 1.6	5.1 ± 1.1	1.3 ± 0.4	0.77 ± 0.21#	0.15 ± 0.06*	0.27 ± 0.08#	0.27 ± 0.10*
140–210	9.2 ± 1.5	5.5 ± 1.4	1.4 ± 0.5	0.79 ± 0.21#	0.13 ± 0.05	0.21 ± 0.04#	0.23 ± 0.07
70–140	8.7 ± 1.9	5.2 ± 1.2	1.3 ± 0.3	0.63 ± 0.11#	0.10 ± 0.06	0.19 ± 0.05#	0.19 ± 0.11
40–70	8.0 ± 1.6	5.1 ± 0.9	1.3 ± 0.3	0.54 ± 0.11#	0.07 ± 0.02	0.22 ± 0.09#	0.12 ± 0.04
Dense ceramics	9.3 ± 0.8	5.9 ± 0.9	n.d.	0.39 ± 0.09	n.d.	0.12 ± 0.03	n.d.

Bone volumes and bone volume densities were determined with quantitative histomorphometry using Cavalieri's method. V Def.: volume of the defect; V Cer.: volume of the ceramic material; V Pore: volume of the macropores; V Bone ext.: volume of bone formed outside of the ceramic particles; V bone pores: volume of bone deposited within the macropores; V_v bone ext.: volume density ratio of bone formed outside of the ceramic particles [new bone volume/defect volume-ceramic volume]; V_v bone pores: volume density ratio of bone deposited within the macropores [bone volume in macropores/volume of macropores]. Mean values ± standard deviation are represented ($n = 6$ for each group).
#$p < 0.05$ vs. dense ceramics.
*$p < 0.05$ vs. 40–70 μm.

140 μm (Table IV). A similar trend was observed when the BIC was calculated for the external surface (Table IV).

Since the BIC does not take into account differences in the surface areas of the ceramic materials and is representing a relative parameter, the surface area of the ceramic material and the surface area of newly-formed bone in contact with the material were thus determined for each group. The external surface area of the ceramic material (excluding the surface furnished by the pores) was similar in each group (Table IV), while the internal surface area of the ceramic material increased with decreasing pore size. However, independently of increasing internal surface areas of ceramics with small pores, the surface area of newly-formed bone was larger in association with ceramic particles whose pore sizes exceeded 140 μm.

A strong positive correlation existed between the BIC for the macropores of the ceramic material and FCD ($R^2 = 0.92$, $p < 0.001$). Albeit less strong, a positive correlation also existed between the volume of newly-formed bone deposited within the macropores of the ceramic material and FCD ($R^2 = 0.66$, $p < 0.001$) (Fig. 4). Twenty-eight days after surgery, the control defects had not undergone spontaneous repair (Fig. 5), thereby confirming that the 4-mm-diameter lesions were of critical size.

DISCUSSION

Angiogenesis, which ultimately leads to functional vascularization, is crucial for bone formation and for the substitution of biomaterials with osseous tissue.

TABLE IV
BIC Ratios and Surface Areas of Newly-Formed Bone Associated With the Ceramic Materials Bearing Pores of Different Sizes, 28 days after Implantation

Pore Size (μm)	BIC Ext. (%)	BIC Pores (%)	Sa Cer. Ext (mm^2)	Sa Cer. Pores (mm^2)	Sa Bone Ext. (mm^2)	Sa Bone pores (mm^2)
210–280	38.0 ± 9.8#,*,**	24.3 ± 6.3*,**	42.3 ± 9.1	41.4 ± 13.7*	16.0 ± 4.6#,*	10.0 ± 4.1*,**
140–210	31.8 ± 6.3	19.7 ± 3.5*,**	50.7 ± 6.7	44.7 ± 16.0*	16.2 ± 3.9#,*	9.1 ± 4.2*,**
70–140	26.0 ± 7.3	8.9 ± 2.4	48.4 ± 12.2	51.7 ± 13.0	11.9 ± 1.7	4.5 ± 1.2
40–70	25.4 ± 6.6	6.4 ± 2.9	40.8 ± 8.0	68.7 ± 17.7	10.4 ± 3.5	4.4 ± 2.1
Dense ceramics	21.0 ± 3.7	n.d.	43.8 ± 4.8	n.d.	9.2 ± 1.9	n.d.

The BIC ratio and the surface areas of the ceramics and of newly-formed bone were quantified histomorphometrically. BIC ext.: BIC ratio for the external surface of the ceramic particles, expressed as a percentage; BIC pores: BIC ratio for the macropore surface, expressed as a percentage; Sa Cer. ext.: surface area of the ceramic particles, excluding the macropores; Sa Cer. pores: surface area of the macropores; Sa Bone ext.: surface area of newly-formed bone in contact with the outside of the ceramic particles (viz., excluding the macropores); Sa Bone pores: surface area of newly-formed bone contacting the macropore surface. Mean values (± standard deviation) are represented ($n = 6$ for each group).
#$p < 0.05$ vs. dense ceramics.
*$p < 0.05$ vs. 40–70 μm.
**$p < 0.05$ vs. 70–140 μm.

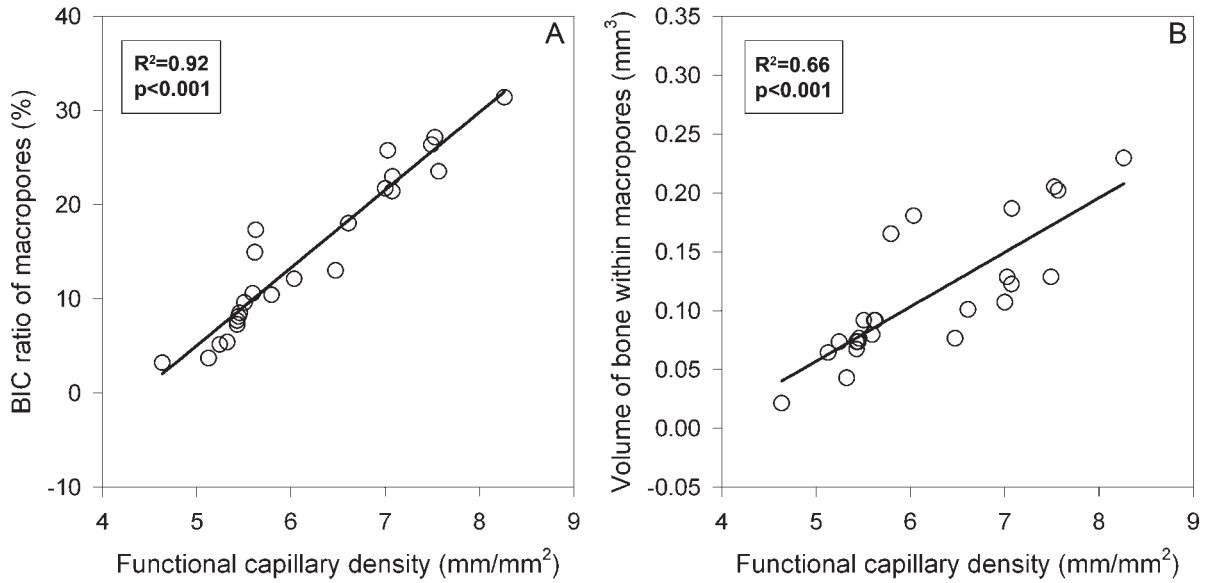

Figure 4. Graphs depicting the correlations existing between FCD (*x*-axes) and either (A) the BIC ratio of the macropores of the ceramic material ($R^2 = 0.92$, $p < 0.001$) or (B) the volume of bone deposited within the macropores ($R^2 = 0.66$, $p < 0.001$). The correlation between the sets of data were statistically analyzed by calculating Pearson's product moment.

Porous bone substitutes permit vessel ingrowth and thus facilitate osteogenesis. Since the pore size of bone substitutes may be a limiting factor for the ingrowth of sprouting capillaries and osseous tissue, we investigated the influence of this parameter on vascularization and bone formation.

As a biomaterial, we used particles of a biphasic calcium phosphate ceramic with different pore sizes. A newly established cranial window preparation in *Balb/c* mice served as our model, and the calvarium as the site for implantation. For a reliable investigation of osseointegration, the biomaterial needs to be implanted into defects that do not heal spontaneously, namely into critical-sized lesions. Aalami et al.[20] have demonstrated that in adult mice, 4-mm-diameter cranial defects do not heal spontaneously during a course of 8 weeks. We thus created 4-mm-diameter calvarial defects, which, when left empty, manifested no evidence of spontaneous repair 28 days after surgery. Angiogenesis and vascularization were monitored by intravital microscopy during the first 28 days of implantation, and bone formation by histomorphometry at the end of this monitoring period.

Histological studies on angiogenesis and bone formation within and around biomaterials have revealed the deposition of osseous tissue to be preceded by the ingrowth of blood capillaries.[9,41] Kuboki et al.[9] have shown that the pore size of hydroxyapatite particles exerts a direct influence on angiogenesis and bone formation. When using particles with pore sizes ranging from 90 to 110 μm; cartilage formation was followed by bone formation similar to the process of endochondral bone formation. The pores were first penetrated by mesenchymal stem cells and then filled with cartilage tissue. Blood vessels subsequently invaded the cartilage tissue, and their presence induced the onset of osteogenesis. When using particles with a pore size of 350 μm, the migration of mesenchymal stem cells into the pores was accompanied by vascular invasion, which was followed by intramembranous ossification without detectable cartilage formation.

In our study, intravital microscopy of the implanted ceramics revealed the dynamics of angiogenesis and vascularization to depend upon the pore size of the material. The onset of blood-vessel formation occurred after a shorter time period, and the FCD was higher in association with ceramics whose pore sizes exceeded 140 μm than with either those whose pore sizes were smaller than 140 μm or dense particles. Since angiogenesis and the microcirculation can be influenced by an immune response against an implanted biomaterial,[42,43] we evaluated several microhemodynamic variables and the interaction between leukocytes and the vascular endothelium. For each parameter, similar values were recorded in each experimental group and in the controls. Hence, the observed differences in angiogenesis and vascularization were indeed a function of pore size, and not attributable to variations in host immunoreactivity to the implanted material.

The optimal osteoconductivity of biomaterials is achieved with pore sizes ranging from 300 to 400 μm.[5,6,9,10] The minimum pore size that is required to generate mineralized bone is considered to be 50 μm.[5–7,10] Our findings are consistent with these data. Ceramics with pore sizes in the range 40–70 μm supported bone formation, and the volume of osseous

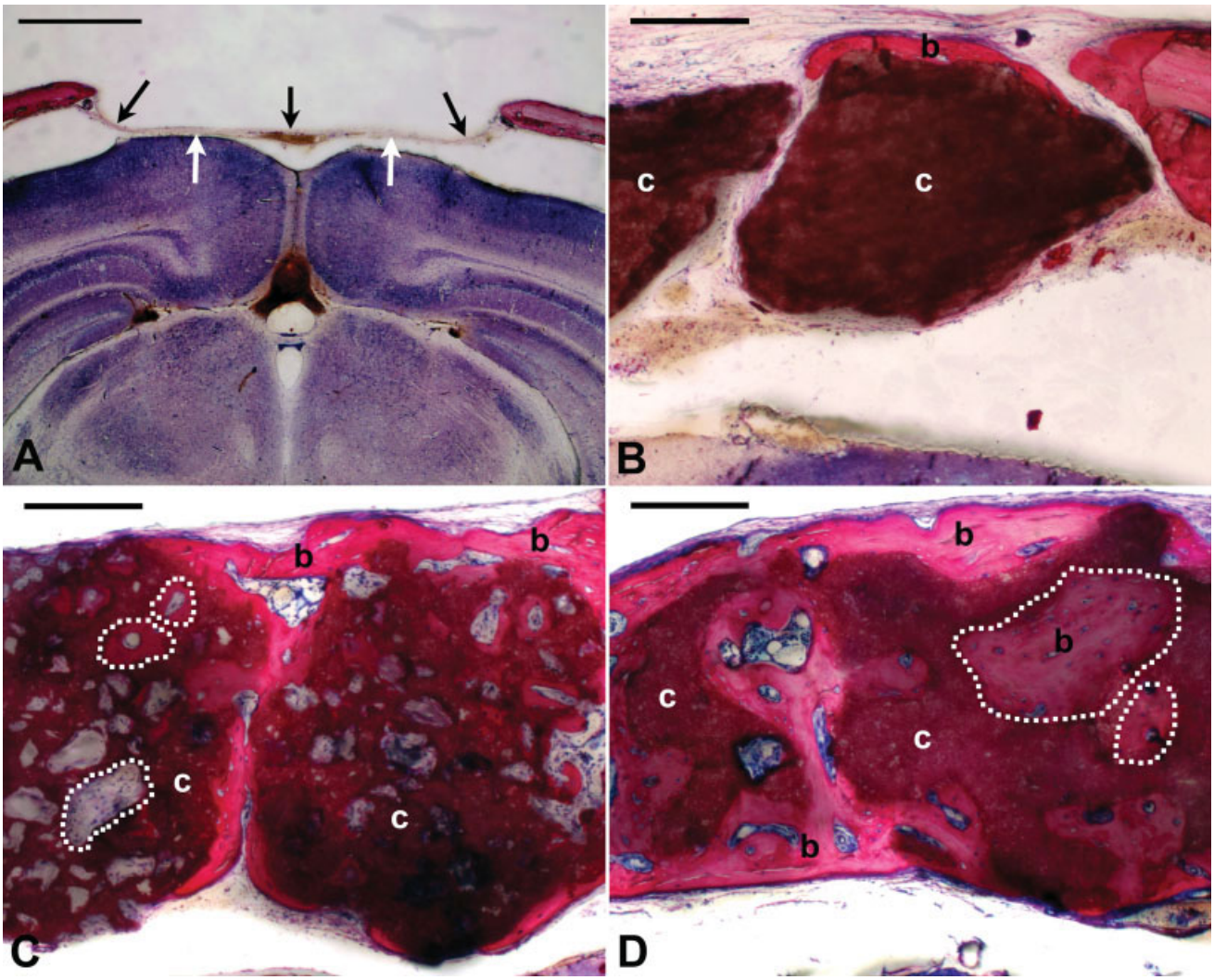

Figure 5. Light micrographs of 300-μm-thick vertical sections through cranial defects, 28 days after surgery. The sections were surface-stained with McNeal's tetrachrome. Ceramic particles (c): brown/red; newly-formed bone (b): light pink; pre-existing bone of the calvarium [visible only in (A)]: magenta; grey matter of the brain: blue/violet. (A) Control (untreated) defect without implantation of ceramic particles. The lesion has not undergone spontaneous repair. The defect has been lined with a thin layer of connective tissue (black/white arrows). (B) Dense ceramic particles. Only small quantities of bone (b) have been deposited sporadically on and around the particles (c). (C) Ceramic particles with pores in the size range 40–70 μm. These particles (c) have been partially surrounded by newly-formed bone (b). However, the small macropores (three of which are outlined in white) contained only small deposits of newly-formed bone (pink). (D) Ceramic particles with pores in the size range 210–280 μm. These ceramic particles (c) have likewise been surrounded by newly-formed bone. But these large macropores (two of which are outlined in white) have been filled with newly-formed bone (pink) for the most part. Scale bars: (A): 1000 μm; (B, C, D): 200 μm.

tissue deposited within the ceramics increased with increasing pore size.

Recently, the surface area of biphasic calcium phosphate ceramic implants has been shown to influence bone formation at an ectopic (intramuscular) site in goats. Twelve weeks after surgery, higher BIC ratios and larger volumes of newly-formed bone were observed in ceramic particles that had greater surface areas. In terms of macroporosity and pore size, the ceramics were similar. The increase in surface area was achieved by increasing the microporosity (pores < 10 μm). In our study, ceramic particles with larger surface areas were associated not with higher but with lower BIC ratios (both externally and within the macropores) and bone volumes. These discrepant findings may be due to the different sizes of the macropores in each study. In the investigation conducted by Habibovic et al.,[23] the diameters of the macropores ranged from 200 to 400 μm, and their size remained unchanged as the surface area of the material was increased. In our study, the sizes of the macropores ranged from 40 to

280 μm, and downsizing the macropores was associated with an increase in the surface area of the material. Intravital microscopy revealed a reduction in pore size to be associated with a decrease in the vascularization of the material. Furthermore, vascularization was positively correlated with both the volume of newly-formed bone deposited within the macropores and the BIC with the macropores. Although ceramic particles with smaller macropores had larger surface areas, their osteoconductivity was impaired because they were less well vascularized. An amplification of the surface area of a material without reducing the size of the macropores may have a positive influence on bone formation, but downsizing the macropores to increase the surface area of a material does not appear to be beneficial. If the macropores are too small, vascularization of the biomaterial may be highly constrained, thereby resulting in deficient bone formation and an impaired osseointegration of the implant. At first sight, this explanation does not appear to be tenable for the influence of pore size on bone formation on the outside of the ceramic particles. However, since vascularization and bone formation were more pronounced in ceramic particles with larger macropores, the surrounding microenvironment within the implantation site may be likewise more osteogenic. Consequently, the osteogenic response in the vicinity of larger-pored ceramics will also be heightened.

For their optimal osseointegration, bone substitutes should not only facilitate the ingrowth of vessels and osseous tissue but also serve as a mechanically stable scaffold for these processes. Amongst other factors, porosity and pore size have an important influence on the mechanical stability of biomaterials.[44–49] Although larger pores ameliorate vascular ingrowth and bone formation, they compromise mechanical stability.[44,45,49] Scaffolds with a porosity of 32–40% and a median pore size of 210 μm have been shown to have a lower compressive modulus than those with a similar porosity but a median pore size of 100 μm.[45] Due to the opposing effects of pore size on the biological and the mechanical properties of bone substitutes, their structural characteristics must necessarily be a compromise between the support of vascularization and bone formation and a decrease in mechanical strength.

In conclusion, by means of intravital microscopy and histomorphometry, we have demonstrated the pore size of a biphasic calcium phosphate ceramic to be a crucial structural parameter in the vascularization and osseointegration of this material *in vivo*. Downsizing of the macropores reduced the vascularization of the ceramics and the formation of bone therein, and impaired their integration into bone. However, it should be borne in mind that large-pored bone substitutes are mechanically less stable than small-pored ones. Hence, pore size must be adjusted so as to establish a compromise between the biological and the mechanical properties of the material.

References

1. Finkemeier CG. Bone-grafting and bone-graft substitutes. J Bone Joint Surg Am 2002;84A:454–464.
2. Kessler S, Mayr-Wohlfart U, Ignatius A, Puhl W, Claes L, Gunther KP. The impact of bone morphogenetic protein-2 (BMP-2), vascular endothelial growth factor (VEGF) and basic fibroblast growth factor (b-FGF) on osseointegration, degradation and biomechanical properties of a synthetic bone substitute. Z Orthop Ihre Grenzgeb 2003;141:472–480.
3. Street J, Bao M, deGuzman L, Bunting S, Peale FV Jr, Ferrara N, Steinmetz H, Hoeffel J, Cleland JL, Daugherty A, van Bruggen N, Redmond HP, Carano RA, Filvaroff EH. Vascular endothelial growth factor stimulates bone repair by promoting angiogenesis and bone turnover. Proc Natl Acad Sci U S A 2002;99:9656–9661.
4. Tarkka T, Sipola A, Jamsa T, Soini Y, Yla-Herttuala S, Tuukkanen J, Hautala T. Adenoviral VEGF-A gene transfer induces angiogenesis and promotes bone formation in healing osseous tissues. J Gene Med 2003;5:560–566.
5. Bobyn JD, Pilliar RM, Cameron HU, Weatherly GC. The optimum pore size for the fixation of porous-surfaced metal implants by the ingrowth of bone. Clin Orthop Relat Res 1980:263–270.
6. Chang BS, Lee CK, Hong KS, Youn HJ, Ryu HS, Chung SS, Park KW. Osteoconduction at porous hydroxyapatite with various pore configurations. Biomaterials 2000;21:1291–1298.
7. Itala AI, Ylanen HO, Ekholm C, Karlsson KH, Aro HT. Pore diameter of more than 100 μm is not requisite for bone ingrowth in rabbits. J Biomed Mater Res 2001;58:679–683.
8. Kuboki Y, Takita H, Kobayashi D, Tsuruga E, Inoue M, Murata M, Nagai N, Dohi Y, Ohgushi H. BMP-induced osteogenesis on the surface of hydroxyapatite with geometrically feasible and nonfeasible structures: topology of osteogenesis. J Biomed Mater Res 1998;39:190–199.
9. Kuboki Y, Jin Q, Takita H. Geometry of carriers controlling phenotypic expression in BMP-induced osteogenesis and chondrogenesis. J Bone Joint Surg Am 2001;83A(Suppl 1): S105–S115.
10. Tsuruga E, Takita H, Itoh H, Wakisaka Y, Kuboki Y. Pore size of porous hydroxyapatite as the cell-substratum controls BMP-induced osteogenesis. J Biochem (Tokyo) 1997;121:317–324.
11. Leunig M, Messmer K. Intravital microscopy in tumor biology: Current status and future perspectives (review). Int J Oncol 1995:413–417.
12. Menger MD, Lehr HA. Scope and perspectives of intravital microscopy—Bridge over from in vitro to in vivo. Immunol Today 1993;14:519–522.
13. Sckell A, Leunig M. Dorsal skinfold chamber preparation in mice. Methods Mol Med 1999;46:95–105.
14. Farhadi MR, Capelle HH, Erber R, Ullrich A, Vajkoczy P. Combined inhibition of vascular endothelial growth factor and platelet-derived growth factor signaling: Effects on the angiogenesis, microcirculation, and growth of orthotopic malignant gliomas. J Neurosurg 2005;102:363–370.
15. Ishikawa M, Kajimura M, Adachi T, Maruyama K, Makino N, Goda N, Yamaguchi T, Sekizuka E, Suematsu M. Carbon monoxide from heme oxygenase-2 Is a tonic regulator against NO-dependent vasodilatation in the adult rat cerebral microcirculation. Circ Res 2005;97:e104–e114.

16. Klenke FM, Gebhard MM, Ewerbeck V, Abdollahi A, Huber PE, Sckell A. The selective Cox-2 inhibitor Celecoxib suppresses angiogenesis and growth of secondary bone tumors: An intravital microscopy study in mice. BMC Cancer 2006; 6:9.
17. Klenke FM, Abdollahi A, Bertl E, Gebhard MM, Ewerbeck V, Huber PE, Sckell A. Tyrosine kinase inhibitor SU6668 represses chondrosarcoma growth via antiangiogenesis in vivo. BMC Cancer 2007;7:49.
18. Vajkoczy P, Farhadi M, Gaumann A, Heidenreich R, Erber R, Wunder A, Tonn JC, Menger MD, Breier G. Microtumor growth initiates angiogenic sprouting with simultaneous expression of VEGF, VEGF receptor-2, and angiopoietin-2. J Clin Invest 2002;109:777–785.
19. Yuan H, Gaber MW, McColgan T, Naimark MD, Kiani MF, Merchant TE. Radiation-induced permeability and leukocyte adhesion in the rat blood–brain barrier: Modulation with anti-ICAM-1 antibodies. Brain Res 2003;969:59–69.
20. Aalami OO, Nacamuli RP, Lenton KA, Cowan CM, Fang TD, Fong KD, Shi YY, Song HM, Sahar DE, Longaker MT. Applications of a mouse model of calvarial healing: Differences in regenerative abilities of juveniles and adults. Plast Reconstr Surg 2004;114:713–720.
21. Krebsbach PH, Mankani MH, Satomura K, Kuznetsov SA, Robey PG. Repair of craniotomy defects using bone marrow stromal cells. Transplantation 1998;66:1272–1278.
22. Peng H, Wright V, Usas A, Gearhart B, Shen HC, Cummins J, Huard J. Synergistic enhancement of bone formation and healing by stem cell-expressed VEGF and bone morphogenetic protein-4. J Clin Invest 2002;110:751–759.
23. Habibovic P, Yuan H, van der Valk CM, Meijer G, van Blitterswijk CA, de Groot K. 3D microenvironment as essential element for osteoinduction by biomaterials. Biomaterials 2005;26:3565–3575.
24. Yuan H, Yang Z, De Bruijn JD, de Groot K, Zhang X. Material-dependent bone induction by calcium phosphate ceramics: A 2.5-year study in dog. Biomaterials 2001;22:2617–2623.
25. Yuan H, van den Dool M, Li S, van Blitterswijk CA, de Groot K, De Bruijn JD. A comparison of the osteoinductive potential of two calcium phosphate ceramics implanted intramuscularly in goats. J Mater Sci Mater Med 2002;13:1271–1275.
26. Forbes H.S. Cerebral circulation. I. Observation and measurement of pial vessels. Arch Neurol Psychiat 1928;19:749–761.
27. Klenke FM, Merkle T, Fellenberg J, Abdollahi A, Huber PE, Gebhard MM, Ewerbeck V, Sckell A. A novel model for the investigation of orthotopically growing primary and secondary bone tumours using intravital microscopy. Lab Anim 2005;39:377–383.
28. Levasseur JE, Wei EP, Raper AJ, Kontos AA, Patterson JL. Detailed description of a cranial window technique for acute and chronic experiments. Stroke 1975;6:308–317.
29. Yuan F, Salehi HA, Boucher Y, Vasthare US, Tuma RF, Jain RK. Vascular permeability and microcirculation of gliomas and mammary carcinomas transplanted in rat and mouse cranial windows. Cancer Res 1994;54:4564–4568.
30. Hoffmann JN, Vollmar B, Laschke MW, Inthorn D, Fertmann J, Schildberg FW, Menger MD. Microhemodynamic and cellular mechanisms of activated protein C action during endotoxemia. Crit Care Med 2004;32:1011–1017.
31. Menger MD, Steiner D, Messmer K. Microvascular ischemia-reperfusion injury in striated muscle: Significance of "no reflow". Am J Physiol 1992;263:H1892–H1900.
32. Nolte D, Zeintl H, Steinbauer M, Pickelmann S, Messmer K. Functional capillary density: An indicator of tissue perfusion. Int J Microcirc Clin Exp 1995;15:244–249.
33. Rucker M, Laschke MW, Junker D, Carvalho C, Schramm A, Mulhaupt R, Gellrich NC, Menger MD. Angiogenic and inflammatory response to biodegradable scaffolds in dorsal skinfold chambers of mice. Biomaterials 2006;27:5027–5038.
34. Sckell A, Safabakhsh N, Dellian M, Jain RK. Primary tumor size-dependent inhibition of angiogenesis at a secondary site: An intravital microscopic study in mice. Cancer Res 1998; 58:5866–5869.
35. Kuhnle GE, Kuebler WM, Groh J, Goetz AE. Effect of blood flow on the leukocyte-endothelium interaction in pulmonary microvessels. Am J Respir Crit Care Med 1995;152:1221–1228.
36. Erben RG. Embedding of bone samples in methylmethacrylate: An improved method suitable for bone histomorphometry, histochemistry, and immunohistochemistry. J Histochem Cytochem 1997;45:307–313.
37. MacNeal WJ. Tetrachrome blood stain: An economical and satisfactory imitation of Leishman's stain. J Am Med Assoc 1922;78:1122–1123.
38. Penney DP, Powers JP, Frank M, Willis C, Churukian C. Analysis and testing of biological stains—The Biological Stain Commission Procedures. Biotech Histochem 2002;77:237–275.
39. Gundersen HJ, Jensen EB. The efficiency of systematic sampling in stereology and its prediction. J Microsc 1987;147:229–263.
40. Baddeley AJ, Gundersen HJ, Cruz-Orive LM. Estimation of surface area from vertical sections. J Microsc 1986;142:259–276.
41. Schmid J, Wallkamm B, Hammerle CH, Gogolewski S, Lang NP. The significance of angiogenesis in guided bone regeneration. A case report of a rabbit experiment. Clin Oral Implants Res 1997;8:244–248.
42. Laschke MW, Haufel JM, Thorlacius H, Menger MD. New experimental approach to study host tissue response to surgical mesh materials in vivo. J Biomed Mater Res A 2005; 74:696–704.
43. Sung HJ, Meredith C, Johnson C, Galis ZS. The effect of scaffold degradation rate on three-dimensional cell growth and angiogenesis. Biomaterials 2004;25:5735–5742.
44. Bignon A, Chouteau J, Chevalier J, Fantozzi G, Carret JP, Chavassieux P, Boivin G, Melin M, Hartmann D. Effect of micro- and macroporosity of bone substitutes on their mechanical properties and cellular response. J Mater Sci Mater Med 2003;14:1089–1097.
45. Borden M, El Amin SF, Attawia M, Laurencin CT. Structural and human cellular assessment of a novel microsphere-based tissue engineered scaffold for bone repair. Biomaterials 2003; 24:597–609.
46. Burdick JA, Frankel D, Dernell WS, Anseth KS. An initial investigation of photocurable three-dimensional lactic acid based scaffolds in a critical-sized cranial defect. Biomaterials 2003;24:1613–1620.
47. Karageorgiou V, Kaplan D. Porosity of 3D biomaterial scaffolds and osteogenesis. Biomaterials 2005;26:5474–5491.
48. Porter BD, Oldham JB, He SL, Zobitz ME, Payne RG, An KN, Currier BL, Mikos AG, Yaszemski MJ. Mechanical properties of a biodegradable bone regeneration scaffold. J Biomech Eng 2000;122:286–288.
49. Zhang Y, Zhang M. Three-dimensional macroporous calcium phosphate bioceramics with nested chitosan sponges for load-bearing bone implants. J Biomed Mater Res 2002;61:1–8.